

Titin-truncating variants in hiPSC cardiomyocytes induce pathogenic proteinopathy and sarcomere defects with preserved core contractile machinery

Guanyi Huang,^{1,5,*} Anjali Bisaria,¹ Devin L. Wakefield,¹ Tracy M. Yamawaki,¹ Xin Luo,¹ Jingli A. Zhang,^{1,4} Patrick Vigneault,^{2,6} Jinghong Wang,² Jeffrey D. Reagan,² Oliver Oliverio,¹ Hong Zhou,¹ Chi-Ming Li,¹ Olaia F. Vila,¹ Songli Wang,¹ Fady I. Malik,³ James J. Hartman,³ and Christopher M. Hale^{1,*}

¹Research Biomics, Amgen Discovery Research, South San Francisco, CA 94080, USA

²Department of Cardiometabolic Disorders, Amgen Discovery Research, South San Francisco, CA 94080, USA

³Research and Development, Cytokinetics, Inc., South San Francisco, CA 94080, USA

⁴Present address: A2 Biotherapeutics, Agoura Hills, CA 91301, USA

⁵Present address: Department of Cardiometabolic Diseases, Merck Research Laboratories, South San Francisco, CA 94080, USA

⁶Present address: Precision Cardiology Lab, Bayer AG, Cambridge, MA 02142, USA

*Correspondence: guanyi.huang@merck.com (G.H.), halec@amgen.com (C.M.H.)

<https://doi.org/10.1016/j.stemcr.2022.11.008>

SUMMARY

Titin-truncating variants (TTNtv) are the single largest genetic cause of dilated cardiomyopathy (DCM). In this study we modeled disease phenotypes of A-band TTNtv-induced DCM in human induced pluripotent stem cell-derived cardiomyocytes (hiPSC-CMs) using genome editing and tissue engineering technologies. Transcriptomic, cellular, and micro-tissue studies revealed that A-band TTNtv hiPSC-CMs exhibit pathogenic proteinopathy, sarcomere defects, aberrant Na⁺ channel activities, and contractile dysfunction. These phenotypes establish a dual mechanism of poison peptide effect and haploinsufficiency that collectively contribute to DCM pathogenesis. However, TTNtv cellular defects did not interfere with the function of the core contractile machinery, the actin-myosin-troponin-Ca²⁺ complex, and preserved the therapeutic mechanism of sarcomere modulators. Treatment of TTNtv cardiac micro-tissues with investigational sarcomere modulators augmented contractility and resulted in sustained transcriptomic changes that promote reversal of DCM disease signatures. Together, our findings elucidate the underlying pathogenic mechanisms of A-band TTNtv-induced DCM and demonstrate the validity of sarcomere modulators as potential therapeutics.

INTRODUCTION

Dilated cardiomyopathy (DCM) is a common type of myocardial disorder characterized by a dilated left ventricle and impaired systolic function. It is also associated with approximately half of the heart-failure cases in the United States. Among dozens of genes contributing to DCM, titin-truncating variants (TTNtv) constitute approximately 25% of familial cases and 18% of sporadic cases (Roberts et al., 2015; Walsh et al., 2017). The poor clinical outcomes of DCM highlight a pressing need for improved mechanistic understanding of DCM pathogenesis, genetic susceptibility, and possible interactions with medical therapy.

Titin, the largest human protein, is an essential component of the cardiac sarcomere. Homozygous TTNtv is embryonic lethal in genetically engineered rodents, suggesting its necessity in sarcomerogenesis (Gramlich et al., 2009; Schafer et al., 2017). However, the pathogenicity of heterozygous TTNtv has been elusive as evidenced by its prevalence in approximately 1% of the general population (Fatkin and Huttner, 2017; Roberts et al., 2015). It was recently discovered that only TTNtv occurring in constitutive exons are consistently associated with DCM, while disease penetrance and severity are position related, with

distal variants exhibiting worse cardiac functions (Hinson et al., 2015; Roberts et al., 2015; Schafer et al., 2017). Despite these efforts, the exact molecular mechanisms of TTNtv-induced DCM remain incompletely understood, with prevailing theories including haploinsufficiency, inactive protein (loss of function), or poison peptide effect (Fomin et al., 2021; McAfee et al., 2021; Ware and Cook, 2018).

Current therapeutics for DCM have been focused on managing symptoms and reducing adverse events. While a fraction of DCM patients with TTNtv recover systolic function by standard medical therapy, many experience worsening clinical outcomes including arrhythmia and heart failure. Thus, there remains an unmet clinical need to explore new therapies aiming to target the molecular and cellular pathogenesis of TTNtv (Repetti et al., 2019). Sarcomere modulators are one example of small molecules that act directly on their target sarcomere proteins and represent a novel therapeutic approach for improving cardiac function while potentially avoiding adverse effects from current indirect inotropic mechanisms (Malik et al., 2011; Teerlink et al., 2020).

Human induced pluripotent stem cell-derived cardiomyocytes (hiPSC-CMs), together with CRISPR-Cas9



genome editing and three-dimensional (3D) tissue engineering, offer new promising approaches for cardiac disease modeling, mechanistic investigation, and drug testing. In this study, we employed these techniques to study molecular mechanisms and cellular outcomes of TTNtv and explored the validity of treating TTNtv-DCM using sarcomere modulators. Our data showed that TTNtv hiPSC-CMs exhibit pathogenic proteinopathy, Na⁺ channel abnormalities, sarcomere defects, and contractile dysfunction, revealing a dual mechanism of poison peptide effect and haploinsufficiency for DCM pathogenesis. Despite defects in multiple cellular functions, however, we demonstrated that TTNtv hiPSC-CMs preserve an uncompromised core contractile machinery, namely the actin-myosin-troponin-Ca²⁺ complex, and retain the therapeutic efficacy of sarcomere modulators.

RESULTS

Generation of hiPSC-CMs carrying titin-truncating variants

To investigate TTNtv cellular pathology, we performed CRISPR-Cas9 genome editing in hiPSCs to model a single nucleotide deletion leading to non-sense mutation in titin A-band (Figure 1A). Isogenic hiPSCs carrying heterozygous (TTN tv/+) and homozygous (TTN tv/tv) mutations were created by homology-directed repair, with minimal off-target effects as indicated by whole-genome sequencing (Figures 1B and S1A–S1E). Mutant hiPSC lines exhibited normal colony morphology, growth, and uniform expression of pluripotent markers OCT4, NANOG, and TRA-1-60 (Figure S1F). Cytogenetic analysis indicated no karyotypical abnormality from genome editing or clonal expansion (Figure S1G). Cardiomyocyte differentiation was conducted using a monolayer-based protocol by modulating Wnt signaling pathways (Figure 1C) (Lian et al., 2013). Wild-type (WT), TTN tv/+, and TTN tv/tv hiPSC lines all produced high-purity hiPSC-CMs consisting predominantly of cTnT⁺MLC2v⁺ ventricular-like cells (Figures 1D and S1H). Under monolayer culture conditions, WT and TTN tv/+ hiPSC-CMs displayed comparable contraction profiles by imaging-based analysis (Figures 1E and S1I). Notably, TTN tv/tv hiPSC-CMs showed no visible contraction despite comparable cardiac troponin T (cTnT) expression relative to WT cells, indicating a non-functional sarcomere. This was confirmed by TTNtv localization, labeled by titin Z-line- but not M-line-specific antibody, that diffuses throughout the cytoplasm with no recognizable pattern in TTN tv/tv hiPSC-CMs. TTN WT and tv/+ hiPSC-CMs were able to form functional sarcomeres, albeit with varying degrees of sarcomere organization at the cellular level (Figure 1F).

Transcriptomic analysis of TTN tv/+ hiPSC-CMs reveals molecular signatures of DCM pathogenesis

We performed RNA sequencing (RNA-seq) of hiPSC-CMs to explore the molecular mechanisms underlying TTNtv functional defects. Cells were sampled at differentiation days 30, 90, and 150. For both WT and TTN tv/+ cells, day-30 samples displayed higher variations and were clustered distinctly in principal component analysis (PCA), which contrasted with day-90 and day-150 samples whose replicates resided in proximity and separated clearly among time points and genotypes (Figure 2A). Time-point-paired analysis indicated a significantly higher proportion of differentially expressed genes (DEGs) exclusive to day-30 populations (Figures 2B and S2A; Table S1). This likely reflects carry-over heterogeneity from cardiac differentiation and a varied degree of immaturity in day-30 hiPSC-CMs. To better understand how hiPSC-CM transcriptome evolves with extended *in vitro* culture, we cross-compared to generate shared gene clusters in which expression changed similarly over time in both WT and mutant cells (temporal DEGs, Figure S2B and Table S2). Upregulated genes showed significant enrichment for gene ontology (GO) terms related to heart contraction and ion transport, indicating an improvement of cardiac physiology and maturation status in long-term culture (Figure 2C).

We next performed hierarchical clustering of DEGs across all time points to identify molecular signatures of the TTN tv/+ genotype (false discovery rate [FDR] < 0.001, Figure 2D and Table S1). GO analysis demonstrated that multiple pathways involved in cardiac contraction and mitochondrial function were selectively downregulated in TTN tv/+ hiPSC-CMs (Figure 2E). This was further validated by Ingenuity Pathway Analysis (IPA) that revealed significant perturbations of gene sets in cardiac arrhythmia, dilated cardiomyopathy, and energy metabolism (Figures 2F and S2C–S2E). Genes related to cardiac fibrosis and remodeling were upregulated as typically observed in DCM (Figures 2E and 2F) (Deacon et al., 2019; Verdonschot et al., 2018). The expression of key cardiomyocyte genes in TTN tv/+ cells further predicted aberrations in multiple functional categories (Figure 2G). We observed decreased expression of sarcomere structural and regulatory genes (MYL2, MYL3, MYH7, LMOD3, FHL2, and MYLK3), and increased expression of secretory stress markers. In addition, STRING network mapping of selected DEGs in Figure 2G showed that titin predominantly interacts with sarcomere proteins, especially MYL2 (and MYL3), which regulates contractility through phosphorylation by MYLK3 (Figure 2H, blue circle). Immunoblotting confirmed dramatically reduced expression of MYL2, MYL3, and LMOD3 but not other sarcomeric proteins (Figure 2I), which agrees with the notion that titin A-band stabilizes the titin-thick filament interaction (Gigli et al., 2016).

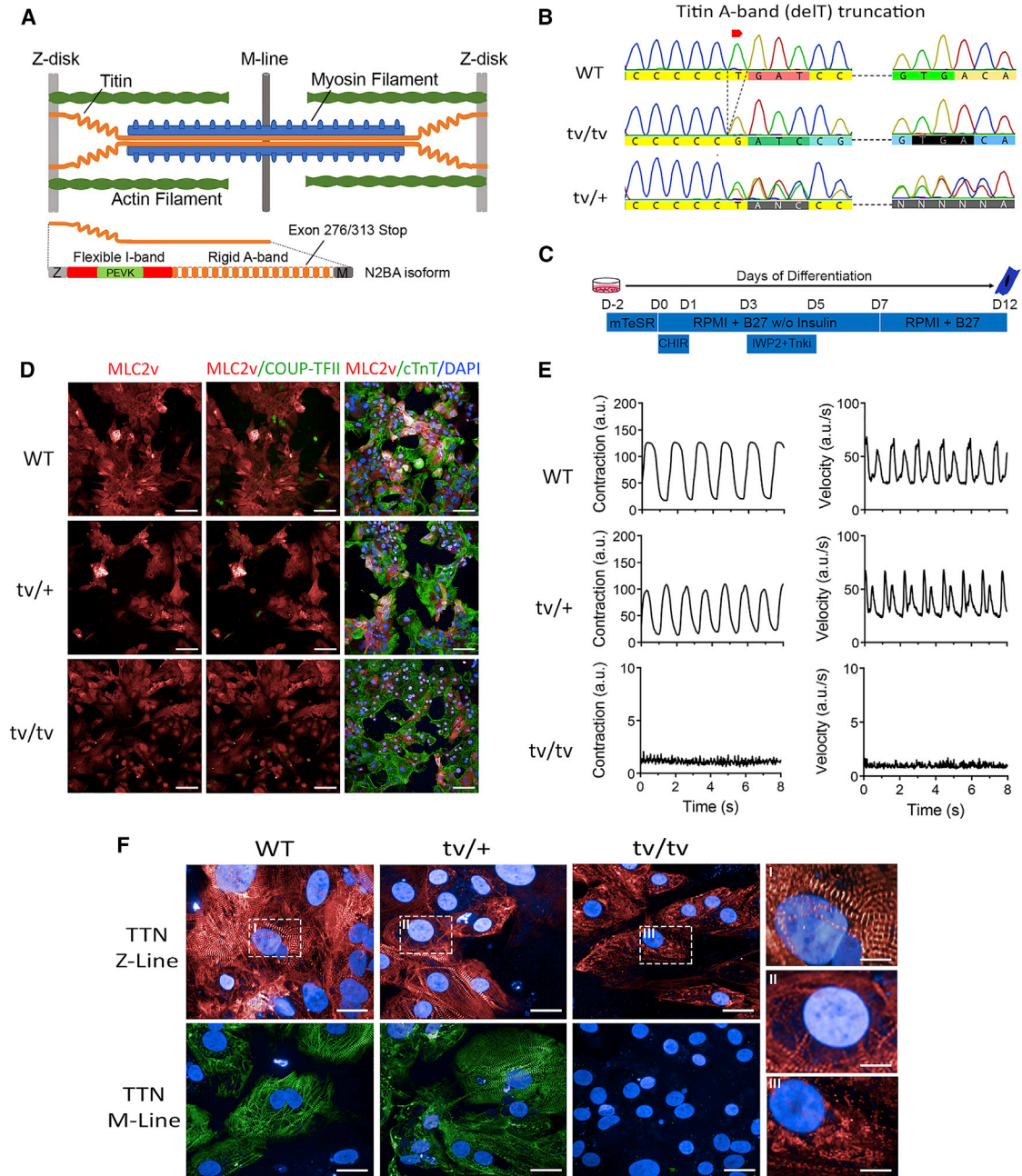


Figure 1. Generation of hiPSC-CMs carrying titin-truncating variants

(A) Schematic representation of one cardiac sarcomere unit with major components.

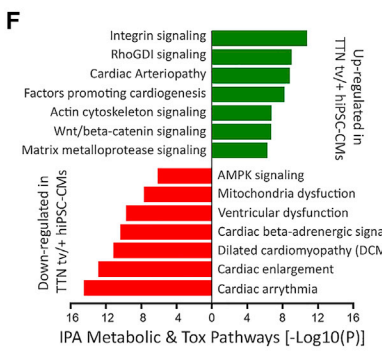
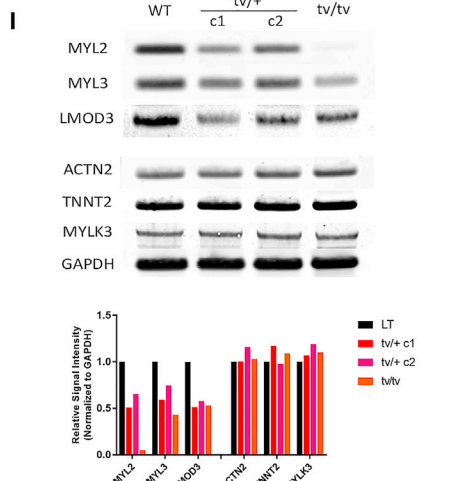
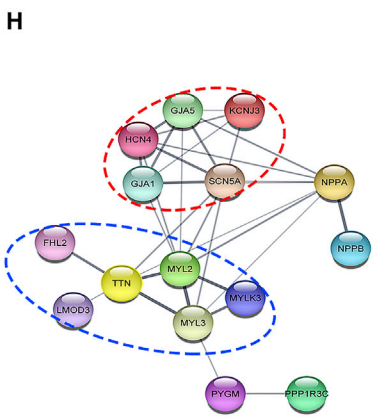
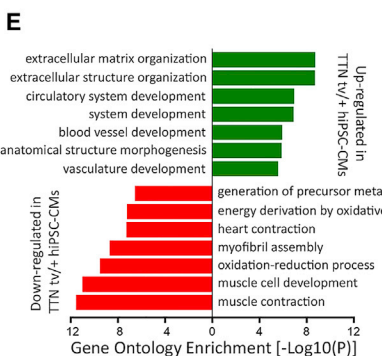
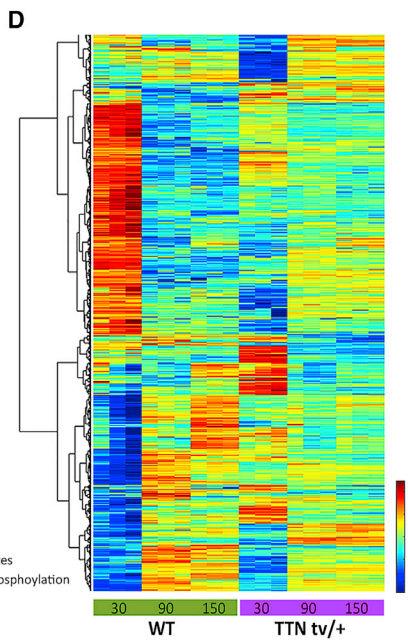
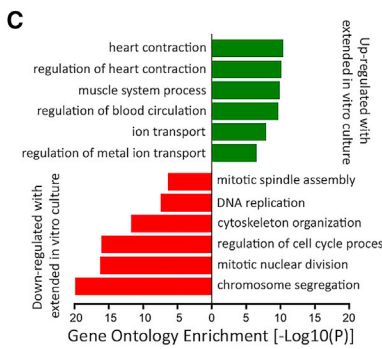
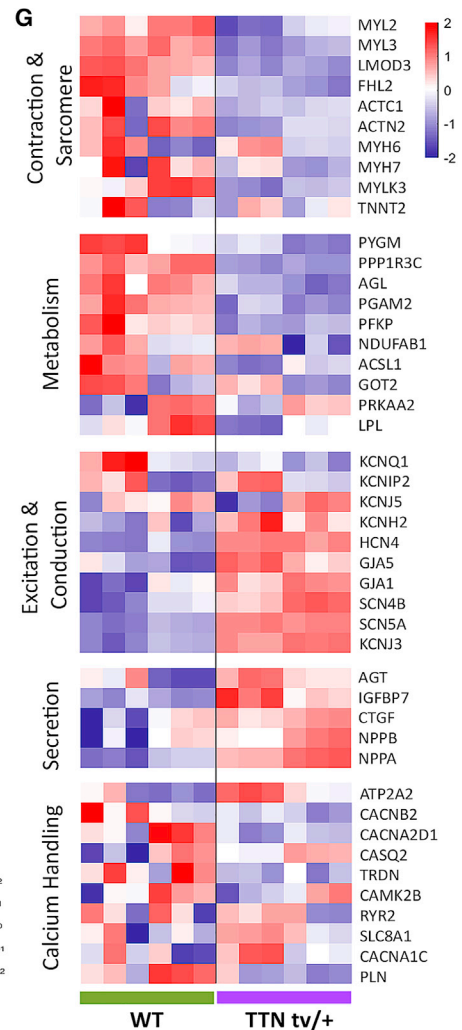
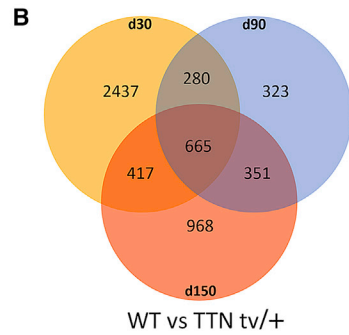
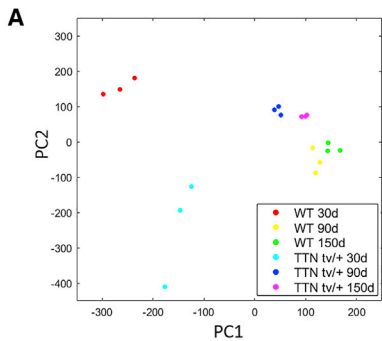
(B) Sanger sequencing confirming the generation of titin A-band truncation hiPSCs.

(C) Schematic workflow of hiPSC cardiac differentiation.

(D) CM differentiation in WT and TTNtv mutant hiPSCs: ventricular (MLC2v), atrial (COUP-TFII), pan-CM (cTnT), nuclei (Hoechst). Scale bars, 100 μ m.

(E) Contraction profiles of WT and TTNtv mutant hiPSC-CMs by 2D motion tracking analysis. See quantification results in [Figure S1I](#).

(F) Representative titin immunofluorescence images of WT, tv/+, and tv/tv hiPSC-CMs: Z-line specific (red); M-line specific (green); Hoechst (blue). Scale bars, 20 μ m. Panels on the right (I, II, and III) show zoom-in views of boxed areas. Scale bars, 5 μ m.



(legend on next page)



Minimal expression of MYL2 was observed in TTN tv/tv cells, and thus we postulate that the disturbance of the titin-thick filament interaction triggers downregulation and/or degradation of MYL2.

TTNtv accumulates in cytoplasm and induces pathogenic proteinopathy

The transcriptional and translational control of TTNtv remains inconclusive, with contradictory reports (Hinson et al., 2015; Roberts et al., 2015; Schafer et al., 2017; Ware and Cook, 2018). We found increasing titin expression as cardiomyocytes mature *in vitro*, consistent with observations on the global transcriptional level, and comparable levels of total titin transcripts at late time points (Figure 3A). Allele-specific SNP analysis revealed stable transcription of both alleles irrespective of SNP locations to the mutation site (Figures 3B and 3C). There was no evidence for nonsense-mediated mRNA decay (NMD) of the TTNtv allele or compensatory upregulation of the WT allele. The isoform splicing of titin transcripts was also unaltered. WT and mutant hiPSC-CMs maintained a comparable N2BA/N2B ratio, with N2BA predominantly expressed regardless of culture time, indicating a limited degree of maturation of hiPSC-CMs *in vitro* (Figures 3D and S3A).

We next investigated the stability of TTNtv using a combination of titin Z-line- and M-line-specific antibodies (Figures 3E and S3B). TTNtv band migrated closely with titin Cronos/T2 but could only be detected by the Z-line-specific antibody, whereas Cronos/T2 was only labeled by the M-line-specific antibody. The expression of TTNtv protein, for both N2B and N2BA, was comparable with that of full-length titin in tv/+ hiPSC-CMs, ruling out the scenario of accelerated TTNtv degradation by cellular protein quality control of truncated proteins. We further tracked TTNtv by inserting mCherry protein preceding the pre-mature stop codon in TTN tv/+ hiPSC-CMs (Figures 3F and S3C–S3F). As expected, we observed varying degrees of TTNtv-

mCherry fusion protein accumulation in hiPSC-CMs (Figure 3G). TTNtv-mCherry tended to migrate and form perinuclear aggresome-like structures that colocalize with lysosomes (LysoTracker or LAMP1) and autophagosomes (LC3B), suggesting the involvement of the autophagy-lysosomal pathway for TTNtv degradation (Figures 3H and S3G–S3H) (Fomin et al., 2021; McAfee et al., 2021). Surprisingly, we did not observe apparent colocalization between TTNtv aggregates and the 26S proteasome (PSMD3). In fact, TTNtv accumulation flux could be partially disrupted by the treatment of autophagy inhibitor Lys05 but not proteasome inhibitor bortezomib (Figures 3I and S3I). Together, these findings suggest dysregulated titin proteasomal degradation and compensatory elevation of the autophagy pathway to clear TTNtv aggregates. With ample evidence demonstrating the involvement of maladaptive autophagy in cardiomyopathy, cardiac proteinopathy, and heart failure (Bravo-San Pedro et al., 2017; Lavandero et al., 2015), we conclude that dysregulated protein degradation represents a major mechanism underlying TTNtv-DCM pathogenesis (see discussion).

TTN tv/+ hiPSC-CMs exhibit normal Ca²⁺ cycling but aberrant Na⁺ channel activities

We examined the electrophysiological properties of TTN tv/+ hiPSC-CMs, as transcriptomic analysis suggested aberrations in cardiomyocyte excitation and conduction as well as potential risks for cardiac arrhythmia (Figures 2F–2H). WT and TTN tv/+ hiPSC-CMs showed similar Ca²⁺ handling and responded to β -adrenergic stimulation normally (Figures 4A and S4A). Unexpectedly, no aberrant arrhythmia-like Ca²⁺ handling events were observed in mutant cells even under isoproterenol challenge, inconsistent with clinical observations of TTNtv-DCM patients (Ahlberg et al., 2018; Corden et al., 2019; Verdonschot et al., 2018). We next compared their action potential (AP) and field potential (FP) signals using the microelectrode array (MEA)

Figure 2. Transcriptomic profiling reveals DCM disease signature of TTN tv/+ hiPSC-CMs

- (A) PCA analysis of WT and TTN tv/+ hiPSC-CMs with different culture time (days 30, 90, and 150). For each time point, samples from three independent differentiation batches were sequenced.
- (B) Venn diagram showing unique and shared DEGs (FDR < 0.05) in time-point-paired analysis. See also Figure S2A.
- (C) GO biological process terms enriched in hierarchically clustered gene subsets that changed consistently in WT and TTN tv/+ hiPSC-CMs with extended *in vitro* culture time.
- (D) Heatmap showing expression patterns of DEGs (FDR < 0.001) between WT and TTN tv/+ hiPSC-CMs on three time points combined. Color scale represents Z score.
- (E and F) GO biological process terms (E) and IPA metabolic and tox pathway terms (F) enriched in gene clusters from (D).
- (G) Heatmap showing expression patterns of selected genes related to key functional aspects of cardiomyocyte physiology on two later time points (day 90 and day 150). Color scale represents Z score.
- (H) STRING database analysis revealing protein-protein interaction between titin and selected dysregulated genes from (G). Blue circles, sarcomere components; red circles, proteins responsible for excitation and conduction. Darker connecting lines represent increased STRING interaction confidence.
- (I) Western blot showing protein expression of selected genes from (H).

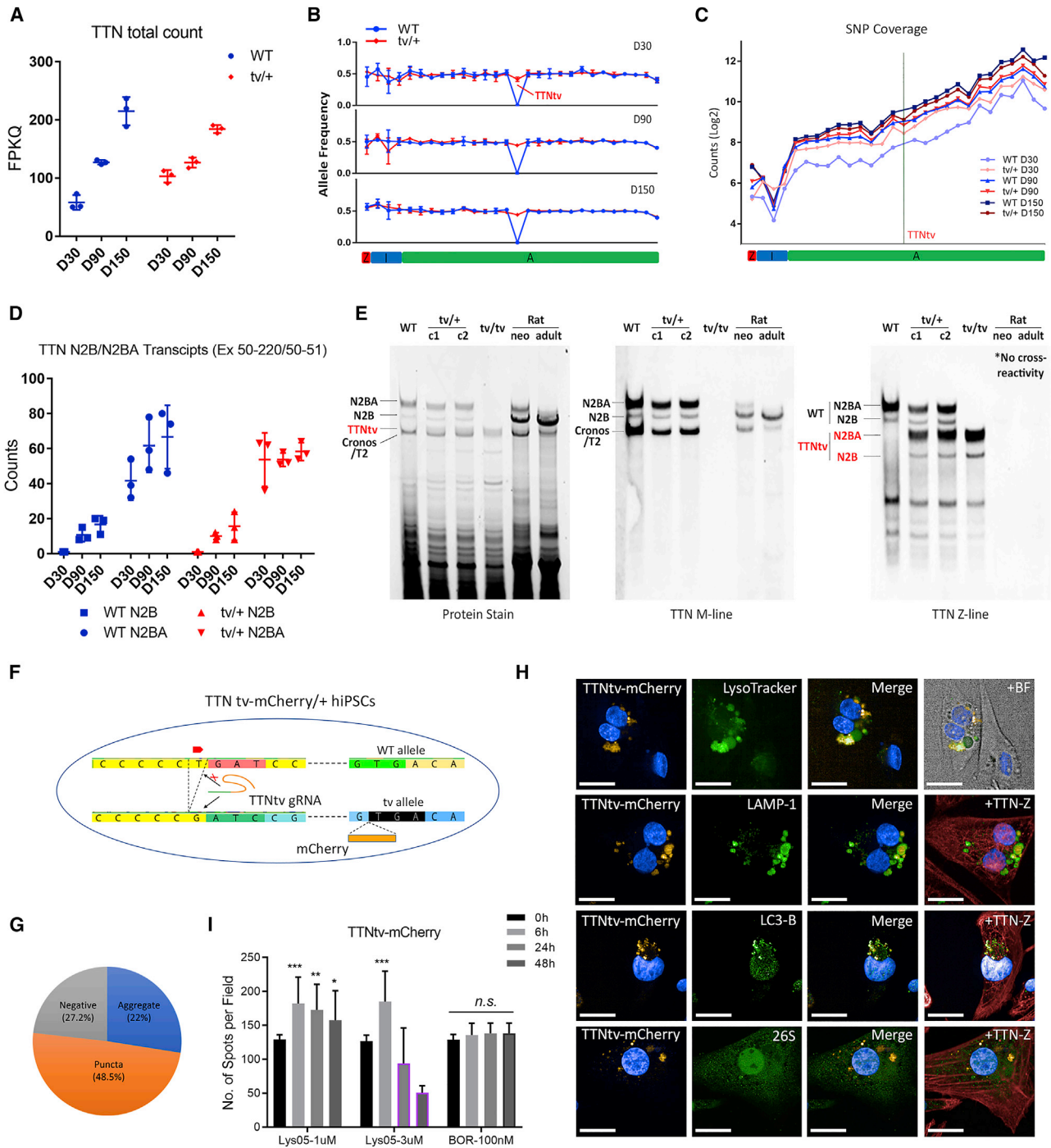


Figure 3. TTNtv accumulates in cytoplasm for autophagy-lysosomal degradation

- (A) Titin total transcript count in WT and TTN tv/+ hiPSC-CMs. Data are shown as mean ± SD.
- (B) Allele frequency of titin transcripts determined by all heterozygous SNPs detected in RNA-seq.
- (C) SNP coverage by log-transformed reads up- and downstream of TTNtv stop codon.
- (D) Titin isoform (N2BA and N2B) transcript count in WT and TTN tv/+ hiPSC-CMs. Isoform-specific exon-exon junction reads were measured: N2B (exons 50–220), N2BA (exons 50–51).
- (E) Protein-stain and titin western blot with Z- and M-specific titin antibodies.
- (F) Gene-targeting strategy to generate TTNtv-mCherry/+ reporter hiPSCs. See also Figures S3C–S3F.

(legend continued on next page)



platform (Figures 4B–4D and S4B–S4D). TTN tv/+ hiPSC-CMs showed prolonged action potential duration (APD₃₀, APD₅₀, and APD₉₀), possibly due to persistent Na⁺ channel activity during the AP plateau that could be arrhythmogenic (Figures 4B and 4C) (Pei et al., 2016; Wan et al., 2016). Consistently, FP recordings showed prolonged FP duration (corrected, FPDc), increased Na⁺ spike amplitude, and decreased spike slopes in TTN tv/+ hiPSC-CMs (Figures 4D and S4B–S4C). TTN tv/+ hiPSC-CMs also displayed desensitization to the treatment of the Na⁺ channel blocker lidocaine (Figure 4E). Treatment with similar compounds, flecainide and mexiletine, confirmed this effect. In comparison, responses to Ca²⁺ channel blockers verapamil and diltiazem were comparable (Figure 4F). Isoproterenol stimulation also had no effect on Na⁺ spike amplitude. Overall, TTN tv/+ hiPSC-CMs maintained normal Ca²⁺ handling properties but displayed aberrant Na⁺ channel activities.

TTN tv/+ hiPSC-CMs display increased sarcomere disorganization and deficiency

Increased sarcomere disorganization is frequently observed in cardiomyopathies associated with genetic mutations (Eschenhagen and Carrier, 2019). We adapted an automated imaging analysis workflow to analyze sarcomere organization at the single-cell level (Figure S5) (Sutcliffe et al., 2018). Late-stage cardiomyocytes were sarcomere-stained and analyzed without manual selection of cells or regions of interest (Figures 5A and S5A–S5C). Cell classification was based on combinations of Haralick correlation features: sarcomere organization score, length, and alignment (Figure 5B, additional examples in Figure S5D). Approximately 3,000 cells were analyzed in each group, and the heterogeneity of cell area, circularity, and aspect ratio were equally represented among cell lines (Figures 5C and S5E). More TTN tv/+ hiPSC-CMs showed disorganized sarcomeres (59.2 versus 36.6% in WT, bottom right quadrant), represented by diffusive sarcomere staining with no clear patterning (Figure 5C): 28.7% of the WT hiPSC-CMs contained a highly organized sarcomere structure (sarcomere length = 1.5–2.2 μm, organization score >0.1, top left quadrant), in comparison with 7.7% of TTN tv/+ cells. Homozygous TTN tv/tv hiPSC-CMs consisted of universally disorganized cells, as observed in Figure 1F.

Previous studies of hiPSC-CMs suggested that aligned sarcomeres were associated with enhanced contractility and maturation metrics (Ribeiro et al., 2015; Yang et al., 2014). In our analysis, WT hiPSC-CMs showed higher levels of favorable sarcomere alignment (smaller angles relative to the major axis of the cell) (Figure 5D). We did not detect a meaningful difference in cell size that has been consistently observed in hypertrophic cardiomyopathy (HCM) but rarely in DCM (Figure S5E) (Eschenhagen and Carrier, 2019). Density distributions of functional sarcomere density and sarcomere coverage showed that TTN tv/+ hiPSC-CMs exhibited reduced sarcomere content and integrity at the single-cell level (Figures 5E, 5F, and S5F). Lastly, in TTN tv-mCherry/+ hiPSC-CMs we identified a positive correlation between TTNtv-mCherry aggregates and disorganized sarcomeres, suggesting that both TTNtv-induced cellular stress and titin haploinsufficiency contribute to sarcomere defects (Figure 5G).

TTN tv/+ hiPSC-CMs show contractile defects in 3D cardiac micro-wires but preserve an intact core contractile machinery and sensitivity to sarcomere modulator therapy

Cardiac contractility is one of the most prominent aspects of heart function and is closely correlated with DCM disease status. We thus developed a 96-well-based 3D cardiac micro-wire (CMW) platform for contractile force measurement (Figures 6A, S6A, and S6B and Video S1) (Thavandiran et al., 2020). Immunostaining of CMWs indicated organized integration of hiPSC-CMs (cTnT) and cardiac fibroblasts (vimentin) (Figure 6B). CMWs exhibited stable contractile force and calcium handling activities, and the dynamic force measurements were validated with known positive (isoproterenol) and negative (blebbistatin) inotropes (Figures S6C–S6F). TTN tv/+ CMWs displayed markedly reduced force, producing only 2.13 ± 1.10 μN (clone 1, n = 148) or 3.20 ± 2.06 μN (clone 2, n = 79), in comparison with 4.84 ± 2.56 μN (n = 105) in WT isogenic controls (Figures 6C and S6G). Kinetic outputs suggested a reduction of contraction and relaxation velocity in TTN tv/+ CMWs, while contraction and relaxation time showed no significant difference (except for a slight increase in relaxation time in tv/+ c2 CMWs) (Figures 6D and 6E). Moreover,

(G) Pie chart showing different sizes of TTNtv-mCherry fusion protein accumulation observed in hiPSC-CM cytoplasm from N = 3 independent differentiation experiments. Size cutoff: negative (<10 pixels²), puncta (10–100 pixels²), aggregate (>100 pixels²). 1 pixel² = 0.036 μm².

(H) Co-staining of TTNtv-mCherry spots with lysosome (LysoTracker and LAMP-1), autophagosome (LC3), and 26S proteasome (PSMD3) markers. Scale bars, 20 μm.

(I) Accumulation of cytoplasmic TTNtv-mCherry spots under autolysosome blocker Lys05 or proteasome inhibitor bortezomib (BOR) treatment. Data are shown as mean ± SD from N = 3 independent experiments. ***p < 0.001; **p < 0.01; *p < 0.05; n.s., not significant; one-way ANOVA with Bonferroni's multiple comparison test. Purple-outlined bars indicate cytotoxicity. See Figure S3I for representative images.

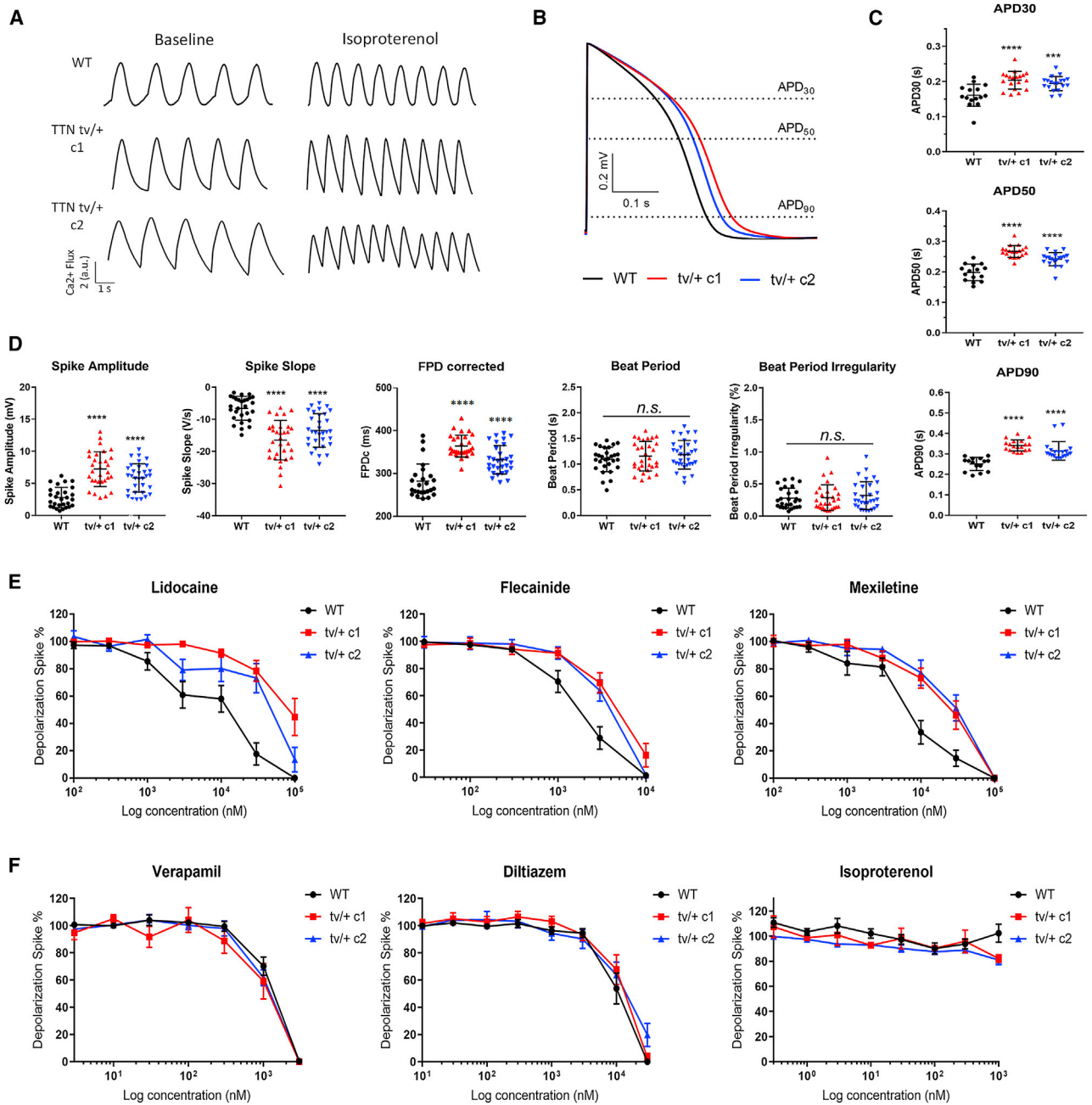


Figure 4. TTN $tv/+$ hiPSC-CMs exhibit normal calcium cycling but aberrant sodium channel activities

(A) Representative Ca^{2+} transients in WT and TTN $tv/+$ hiPSC-CMs. See Figure S4A for quantification of output parameters.

(B) Representative action potential (AP) traces in WT and TTN $tv/+$ hiPSC-CMs (paced at 1.5 Hz) on the multi-electrode array (MEA) platform.

(C and D) Action potential and field potential output parameters. Additional parameters are shown in Figure S4D. Data are shown as mean \pm SD. Each data point represents readings from one well of MEA 96-well plates in N = 3 independent experiments. ****p < 0.0001; ***p < 0.001; n.s., not significant; one-way ANOVA with Bonferroni's multiple comparison test.

(E and F) Pharmacological responses of WT and TTN $tv/+$ hiPSC-CMs. Changes in Na^+ depolarization spike amplitude in field potential recordings are reported. Values are normalized to baseline readings and presented as mean \pm SEM. Data were collected from N = 3 independent experiments.

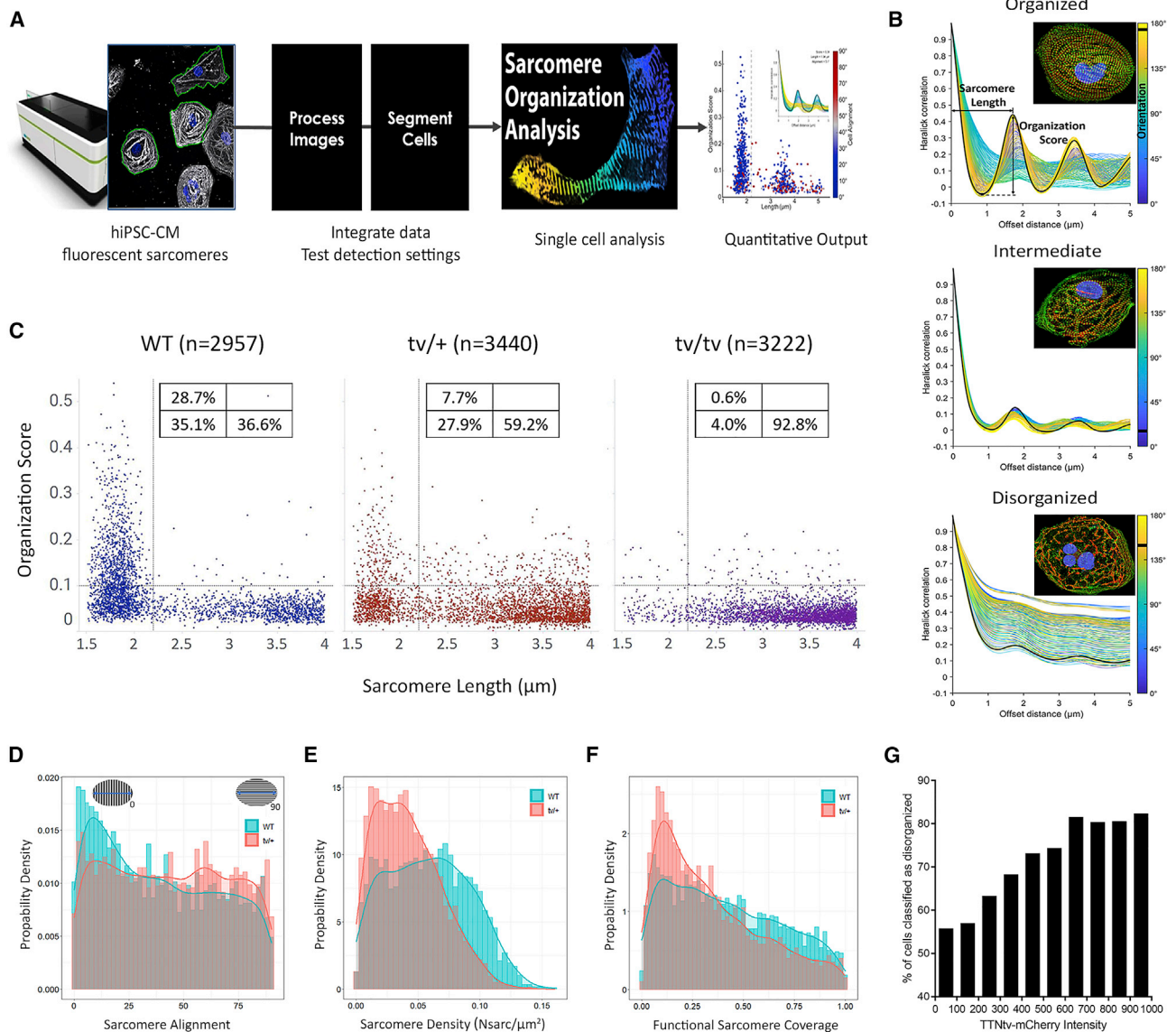


Figure 5. TTN $tv/+$ hiPSC-CMs display sarcomere disorganization and deficiency at single-cell level

(A) Schematic workflow of automated sarcomere organization analysis (SOA).

(B) Representative Haralick plots and SOA analysis outputs of hiPSC-CM sarcomeres. Categorization of sarcomere organization is based on the combinations of sarcomere length, organization score, and sarcomere alignment. Immunofluorescence markers: α -actinin (green), cTnT (red), and Hoechst (blue).

(C) Scatterplots of single-cell SOA analysis of WT, TTN $tv/+$ (clone 1 and clone 2 combined) and TTN tv/tv hiPSC-CMs. Cells were gated on quadrants of organization score and sarcomere length and categorized as exemplified in (B): organized (top left); intermediate (bottom left); and disorganized (bottom right). Percentage values of cells in each quadrant are shown on the plots. n represents the total number of cells analyzed in three independent differentiation experiments.

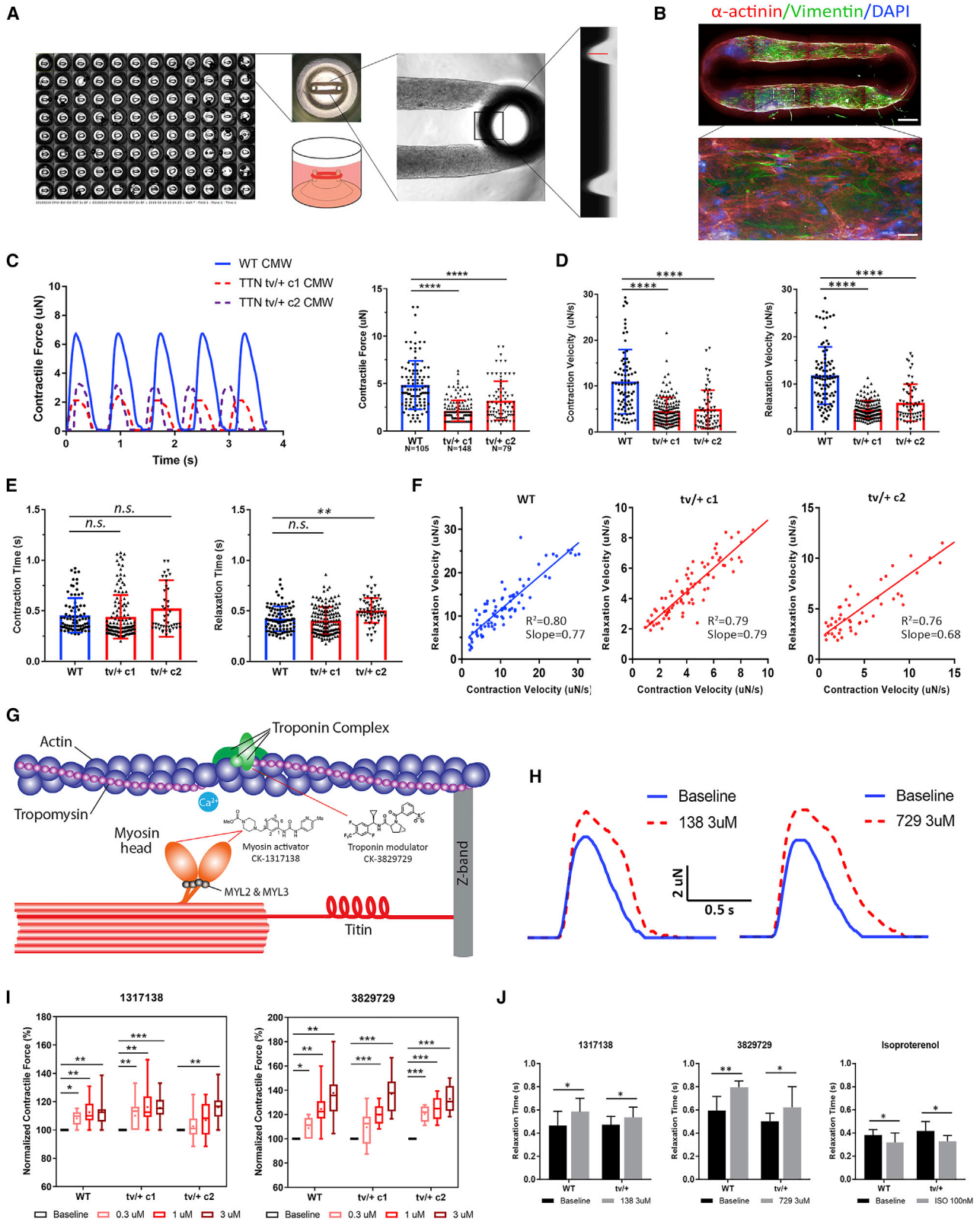
(D) Histogram showing the distribution of sarcomere alignment (0° – 90°) in WT and TTN $tv/+$ hiPSC-CMs.

(E and F) Histogram comparisons of sarcomere density (E) and functional sarcomere coverage (F) between WT and TTN $tv/+$ hiPSC-CMs.

(G) Positive correlation between TTNtv aggregation and sarcomere disorganization: cells with higher TTNtv-mCherry expression showed an increased proportion classified as disorganized.

we observed a consistent correlation between contraction and relaxation velocity for both WT and TTN $tv/+$ CMWs, and the regression slope also suggested a preserved

balance between contraction and relaxation kinetics in TTN $tv/+$ CMWs (Figure 6F). These data demonstrated that TTN $tv/+$ CMWs produce reduced contractile force,



(legend on next page)



likely due to a greater fraction of cells with sarcomere deficiency and disorganization (Figure 5), but maintain intrinsic contraction-relaxation coupling kinetics.

Sarcomere modulators represent a novel therapeutic approach to improve cardiac contraction by directly targeting specific sarcomeric proteins (Hwang and Sykes, 2015). For example, omecamtiv mecarbil is a selective myosin activator that increases contractility by promoting and stabilizing a strong actin-bound force-generating state (Malik et al., 2011; Teerlink et al., 2020). We thus hypothesized that sarcomere modulators are promising therapeutic agents for treating TTNtv-DCM, as they act on existing sarcomeres to augment force generation. We studied the effect of two investigational sarcomere modulators on WT and TTN tv/+ CMWs: one myosin activator (CK-1317138, or 138) that targets the myosin head S1 domain, and one troponin modulator (CK-3829729, or 729) that binds at the interface of troponins C and I (Figure 6G). In dose-escalating CMW studies, we observed a partial rescue of contractile forces with acute treatment of both 138 and 729, with 729 being more efficacious (40% increase of TTNtv contractility at 3 μ M), and no meaningful difference between WT and TTN tv/+ CMWs was detected with either compound (Figures 6H and 6I). Importantly, we found that sarcomere modulator treatment altered the contractile kinetics, as opposed to the phenotype of weakened force but reserved contraction-relaxation kinetic coupling in TTN tv/+ CMWs. 138 or 729 treatment led to decreased contraction time but increased relaxation time (and total peak duration) of CMWs regardless of genotype (Figures 6H, 6J, and S6H). This differs from the effect of β -adrenergic stimulation, as isoproterenol treatment hastened the entire cardiac cellular responses including beat rate, contraction,

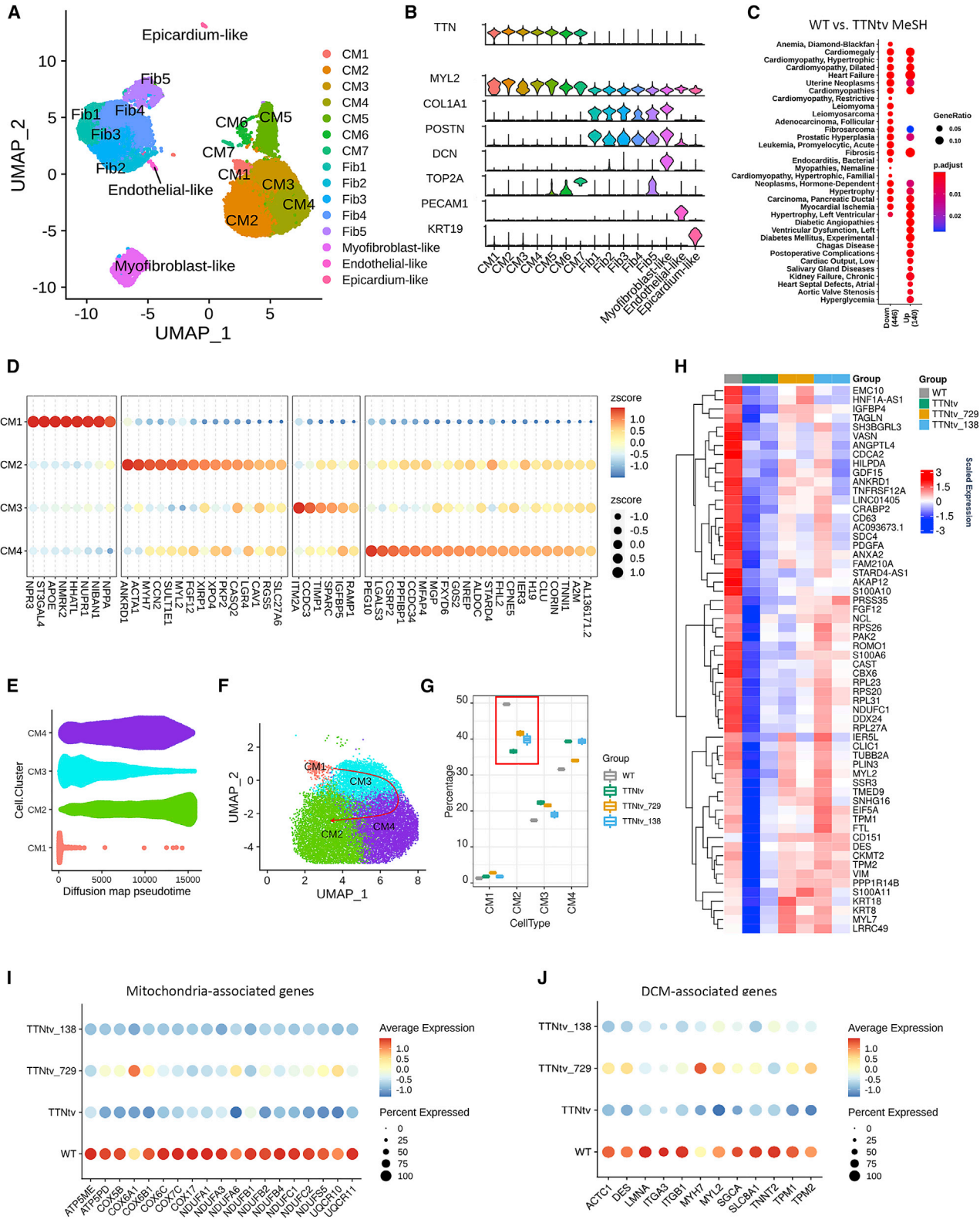
and relaxation time. Sarcomere modulators also did not affect Ca^{2+} transients or Na^+ spike (Figure S6I and Malik et al., 2011). We therefore conclude that TTN tv/+ hiPSC-CMs exhibit intact core contractile machinery and preserve the therapeutic mechanism of sarcomere modulators for improving cardiac contractility.

Sustained sarcomere modulator treatment promotes reversal of TTNtv-DCM disease signatures

It remains unknown as to whether targeting of core contractile machinery by extended exposure to sarcomere modulators can drive persistent transcriptomic changes of cardiomyocytes. To examine this, we treated TTN tv/+ CMWs with 138 or 729 for 14 days and conducted single-cell RNA-seq (scRNA-seq). A total of 29,515 cells were sequenced and 16 clusters were identified, including two major cell types (cardiomyocytes with seven clusters and fibroblasts with five clusters), as well as other minor populations (Figures 7A, 7B, and S7A–S7D). Pathway analysis of DEGs in cardiomyocytes again suggested disease signatures of DCM, consistent with prior bulk RNA-seq results (Figure 7C). Among these clusters, CM1–4 represent the majority of the cardiomyocyte population and are non-proliferative as indicated by cell-cycle analysis (Figures 7A and S7E). CM2 cluster expressed the highest level of sarcomere-associated genes including *MYL2*, *MYH7*, *ACTA1*, *PKP2*, and *ANKRD1*, suggesting increased contractility and/or functional maturity of this cell cluster (Figures 7D and S7G). Indeed, diffusion map pseudotime analysis revealed a trajectory depicting CM2 as the most functionally mature population (Figures 7E, 7F, and S7F). When comparing the CM cluster composition changes among different groups, we found TTNtv CMWs had the lowest percentage

Figure 6. TTN tv/+ CMWs show contractile defects but preserve an intact core contractile machinery for sarcomere modulator therapy

- (A) Illustration of the 3D cardiac micro-wire (CMW) platform for contractility assay.
- (B) Immunofluorescence images of CMW: hiPSC-CMs (α -actinin, red); cardiac fibroblasts (vimentin, green); nuclei (DAPI, blue). Bottom panel shows zoom-in view. Scale bars, 2 mm (top) and 200 μ m (bottom).
- (C–E) Contractile measurements of WT and TTN tv/+ CMWs: (C) representative raw traces (left) and contractile force (right), (D) contraction (left) and relaxation (right) velocity, and (E) contraction (left) and relaxation (right) time. Data are shown as scatterplots with bar graphs representing mean \pm SD. Each data point represents measurements of one CMW from N = 3 independent batches. ****p < 0.0001; **p < 0.01; n.s., not significant; one-way ANOVA with Bonferroni's multiple comparison test.
- (F) Comparison of contractile kinetics between WT and TTN tv/+ CMWs using contraction velocity and relaxation velocity. The coefficient of determination R^2 and linear regression slope are reported.
- (G) The cardiac core contractile machinery and mechanisms of action of sarcomere modulators.
- (H) Representative contractile traces of CMWs at baseline and under treatment of sarcomere modulators: CK-1317138 (left), CK-3829729 (right); the highest dose is shown.
- (I) Increased contractility in WT and TTN tv/+ CMWs under sarcomere modulator treatment. Tissues were acutely exposed to escalating doses of sarcomere modulators and the responses were normalized to baseline. n > 10 CMWs were used for each group and each compound in N = 3 independent experiments. Results are shown as box and whiskers (minimum to maximum) with median (middle lines) and mean (red dots). ***p < 0.001; **p < 0.01; *p < 0.05; two-way ANOVA with Bonferroni's multiple comparison test.
- (J) Changes in CMW relaxation time under sarcomere activators (I) and isoproterenol treatment. Data are shown as mean \pm SD, N = 5; **p < 0.01, *p < 0.05.



(legend on next page)



of CM2 cells, while 138 or 729 treatment resulted in an increased proportion of the CM2 cluster population, albeit still lower than WT CMWs (Figure 7G).

We further identified a subset of 60 genes that showed decreased expression in TTNtv cells but were partially restored by sarcomere modulator treatment (Figure 7H and Table S3). This includes multiple genes (*MYL2*, *MYL7*, *TPM1*, and *TPM2*) involved in actin-myosin filament sliding, suggesting that sarcomere modulators not only acutely augment force generation but also exert positive feedback that increases sarcomere gene expression for improving long-term CM functionality. Among these genes, *MYL2* was also the most significantly downregulated TTNtv gene in our bulk RNA-seq and immunoblotting analysis (Figures 2G and 2I). Moreover, by cross-checking with prior results on TTNtv-DCM phenotypes (Figures 2E, 2F, and S2D), we confirmed the restoration of many mitochondria- and DCM-associated gene signatures in TTNtv CMWs following sarcomere modulator treatment (Figures 7I and 7J). We also noticed a reduction of fibrosis-associated gene signatures, especially in the myofibroblast-like cell cluster, indicating an active interaction between cardiomyocytes and fibroblasts in CMWs (Figure S7H).

DISCUSSION

In this study, we utilized genome-edited hiPSC-CMs and cardiac micro-tissues to investigate the phenotypes and underlying mechanisms of A-band TTNtv-induced DCM (see graphic abstract). TTN tv/+ hiPSC-CMs exhibited reduced expression of genes related to contractility, in line with a previous analysis of samples from patients with DCM-caused heart failure (Wang et al., 2020). Several key sarcomere proteins including *MYL2* were significantly downregulated at both the RNA (bulk RNA-seq and scRNA-seq) and protein level, reflecting defective sarcomere homeostasis. Compared with other abundant sarcomeric

proteins, *MYL2* expression level may be highly indicative of sarcomere (in)sufficiency, as evidenced by its minimal expression in TTN tv/tv hiPSC-CMs. Interestingly, TTNtv mutant hiPSC-CMs express *MYL2* at a normal level during the early cardiac differentiation process (Figure 1D). It is possible that *MYL2* is induced to specify ventricular cardiac fate and then downregulated in TTNtv hiPSC-CMs. The stability of *MYL2* may be dysregulated, as a close physical interaction between *MYL2* and titin A/M-band has been reported (Rudolph et al., 2020). TTN tv/+ hiPSC-CMs also showed an overall lower expression of mitochondrial and metabolic genes, likely due to TTNtv proteinopathy-induced metabolic stress or lower energy demands from reduced contractility. Importantly, sarcomere modulator treatment, beyond its acute positive inotropic effect, was able to restore contractile and mitochondrial gene expression in TTN tv/+ CMWs, indicating a reversal of DCM disease signatures.

Several ion channel and cell junction proteins responsible for cardiomyocyte excitation and conduction showed differential expression in TTN tv/+ hiPSC-CMs. Unexpectedly, we did not detect apparent arrhythmic behaviors in TTN tv/+ hiPSC-CMs (and CMWs, data not shown), despite well-established clinical associations (Ahlberg et al., 2018; Corden et al., 2019; Verdonschot et al., 2018). Several reasons may account for this discrepancy: (1) complex regulation of $\text{Na}_v1.5$ function by its expression level, cytoplasmic trafficking, membrane distribution, and interaction with other proteins; (2) incomplete recapitulation of the electrophysiological apparatus due to hiPSC-CM immaturity; (3) atrial-like hiPSC-CMs may be more suitable for studying atrial fibrillation frequently observed in arrhythmic TTNtv-DCM patients; and (4) arrhythmia due to ventricular remodeling in DCM progression is difficult to model *in vitro*. Nevertheless, at the cellular level, TTN tv/+ hiPSC-CMs displayed aberrant Na^+ channel activities and desensitization to Na^+ channel blockers on the MEA platform. These characteristics are potentially arrhythmogenic under pathophysiological conditions.

Figure 7. Sarcomere modulator-treated TTNtv CMWs indicated reversal of DCM disease signatures

- (A) UMAP projection of CMW cell clusters identified by scRNA-seq ($n = 29,515$) from two independent differentiation batches.
- (B) Violin plot showing normalized expression of representative signature genes of cell clusters.
- (C) List of representative cardiometabolic disease-associated MeSH terms enriched in TTNtv CMW DEGs (CM clusters). The size of the dot reflects the GeneRatio and the color of the dot indicates increasing significance of the enriched pathways. Top 20 significantly enriched terms ($p < 0.05$) are presented.
- (D) Expression patterns of top 50 informative genes in non-dividing cardiomyocyte clusters (CM1–4).
- (E) Bar graph of diffusion map pseudotime component 3 distribution across clusters CM1–4.
- (F) UMAP projection of clusters CM1–4 identified by scRNA-seq ($n = 15,802$). Arrow indicates the direction of cardiomyocyte functional maturity by pseudotime analysis.
- (G) Relative cell composition of clusters CM1–4 across genotypes and treatment groups.
- (H) Heatmap showing expression of representative genes decreased in TTNtv CMWs but restored under sarcomere modulator treatment.
- (I and J) Expression of selected mitochondria-associated genes (I) and DCM-associated genes (J) with decreased expression in TTNtv. The size of the dot indicates the percentage of cells, and the color of the dot represents the scaled average expression level of expressing cells.



Our study agrees with two concurrent publications investigating TTNtv-DCM hearts and hiPSC-CMs: (1) TTNtv allele is actively transcribed without NMD and dosage compensation, and is stably expressed in the CMs; (2) TTNtv haploinsufficiency results in sarcomere deficiency and reduced contractility; and (3) TTNtv protein accumulates as cytoplasmic aggregates and leads to dysregulated protein quality control (PQC) system, suggesting the poison peptide effect as an independent pathogenic mechanism (Fomin et al., 2021; McAfee et al., 2021). However, we noted a difference regarding the relative contributions of proteasome degradation and autophagy pathway in clearing TTNtv aggregates: Fomin et al. reported that proteasome inhibitor treatment led to increased TTNtv content and improved contractile force in engineered heart tissue, while in our study the autophagy-lysosomal pathway plays a more dominant role (Figure 3I) and we did not detect pharmacological rescue from proteasome inhibitor treatment in CMWs (Figure S6J). It is possible that different cell lines have varied baseline activity and/or preference over these two PQC pathways. The cellular abundance of TTNtv may also be relevant, as we observed a much higher level of TTNtv expression (Figure 3E) than reported by Fomin et al. (only 15% of WT titin expression). In addition, the lower ubiquitination level of TTNtv suggests it is an inefficient substrate. We speculate that this is caused by the lack of the C terminus in TTNtv. It was reported that the titin M-band is particularly enriched in lysine residues for ubiquitination (Ryder et al., 2015), and it contains a kinase signaling domain with direct interaction with multiple ubiquitin-proteasome system (UPS)-regulating proteins including TRIM63/MURF1 (an E3 ubiquitin ligase), CAPN3, and FHL2 (Linke and Kruger, 2010). Our RNA-seq data suggested a reduced expression of these genes in TTN tv/+ hiPSC-CMs (Figure S2F), consistent with the observations by Fomin et al. (2021) at the protein level. Therefore, the higher level of TTNtv expression and its inefficient ubiquitination in our cell system will likely saturate the UPS and trigger adaptive macro-autophagy as the main resource for aggregate clearance. This may explain why we did not observe increased contractility in the CMW system under proteasome inhibitor treatment. As the variability of TTNtv content is large among TTNtv-DCM patients, we postulate a combined pharmacological intervention of both PQC pathways may lead to a more promising outcome. This therapeutic strategy may also be explored in other cardiac proteinopathies, including desmin-related cardiomyopathy in which PQC dysregulation leads to pathogenic mitochondrial dysfunction and metabolic defects (McLendon and Robbins, 2011; Shintani-Domoto et al., 2017).

Contractility measurements of two-dimensional (2D) monolayer hiPSC-CMs typically rely on surrogate parameters, including electric impedance and imaging-based mo-

tion tracking analysis. It is unclear whether these readouts are equivalent to contractility force, although they correlate in some interpretations. The 3D micro-tissue platform with post-bending design allows direct force measurement and the detection of TTNtv hiPSC-CM contractile defects not shown in the 2D monolayer setting. This system also incorporated human cardiac fibroblasts to better recapitulate native tissue architecture with improved sarcomere structures and maturation status (Giacomelli et al., 2020; Ronaldson-Bouchard et al., 2018). TTN tv/+ CMWs exhibited a significant reduction of contractile force, in line with observations from transcriptomic profiling and sarcomere organization analysis. Importantly, we noticed a preserved balance between contraction and relaxation kinetics in mutant CMWs. As contraction-relaxation coupling is determined by intrinsic properties of the sarcomere (Jansen, 2019), we believe the core contractile machinery, the actin-myosin-troponin-Ca²⁺ complex, remains uncompromised in TTN tv/+ cells. This reasoning supports the validity of using sarcomere modulators for treating TTNtv-DCM.

In the phase 2 COSMIC-HF clinical trial, the cardiac myosin activator omecamtiv mecarbil improved cardiac function and decreased ventricular diameters in patients with heart failure with reduced ejection fraction, and in the recent phase 3 GALACTIC-HF clinical trial, omecamtiv mecarbil led to a lower risk of a first heart-failure event but did not show a survival benefit (Teerlink et al., 2016, 2020). In patients with lower baseline left ventricular ejection fraction, treatment with omecamtiv mecarbil resulted in greater relative and absolute risk reductions of heart-failure events (Teerlink et al., 2021). In addition to phenotyping patients who might be more responsive to sarcomere modulators, genotyping DCM patients for pathogenic variants could also be important for identifying patients who might benefit from these therapies, as DCM patients bearing sarcomere mutations commonly progress to heart failure. It is thus critically important to investigate whether each of these sarcomere mutations disrupt the core contractile machinery in a way that interferes with the therapeutic mechanism of sarcomere modulators. In this study, we demonstrated that sarcomeres with TTNtv, the most prevalent genetic mutation contributing to DCM and heart failure, retain sensitivity to sarcomere modulations.

EXPERIMENTAL PROCEDURES

Resource availability

Corresponding authors

Guanyi Huang guanyi.huang@merck.com; Christopher Hale halec@amgen.com.

Materials availability

The unique materials generated in this study are available upon reasonable request with a completed material transfer agreement.



Data and code availability

The raw data for the bulk and single-cell RNA-seq data reported in this study have been deposited in the NCBI's Gene Expression Omnibus (GEO: GSE183218). Custom codes for sarcomere organization analysis and CMW contractility analysis will be shared upon reasonable request.

Maintenance and CRISPR-Cas9 genome editing of hiPSCs

hiPSCs (Thermo Fisher, A18945) were maintained on Matrigel-coated (BD Biosciences) tissue culture plates with daily refreshment of mTeSR1 medium (STEMCELL Technologies). Cells were passaged every 3–5 days using ReLeSR (STEMCELL) and supplemented with 10 μ M Y-27532 (Tocris) for the first 24 h following passaging. For CRISPR-Cas9 genome editing, hiPSCs were nucleofected with a mixture of CAS9-RNP and mutation-carrying donor template and screened for single-cell clones with desired genotypes. For details of nucleofection and donor template design, refer to [supplemental information](#).

hiPSC-CM differentiation

WT and mutant hiPSCs were differentiated into ventricular CMs using modifications to a previously published protocol ([Lian et al., 2013](#)). Refer to [supplemental information](#) for details. Differentiated hiPSC-CMs were maintained in RPMI/1640 medium with B27 supplement at the density of 3.6×10^5 cells/cm² with medium changes every 3 days until use.

Cardiac micro-wire studies

For CMW seeding, 96-well custom-fabricated CMW plates were prepared as previously described ([Thavandiran et al., 2020](#)). The ECM Master Mix was prepared fresh as 3 mg/mL Rat Tail Collagen Type I (Corning), 10% Matrigel GFR (Corning), 0.75% NaHCO₃, 0.1 mM NaOH in cold M199 medium. Day-30 hiPSC-CMs and human cardiac fibroblasts (PromoCell) were dissociated into single-cell suspension and mixed as a 90:10 ratio ($0.75\text{--}1 \times 10^5$ cells total per micro-tissue) in 10 μ L of ECM Master Mix per tissue. Automated CMW seeding using liquid handling (Bravo, Agilent) was performed. Medium containing DMEM/F12, 2% fetal bovine serum, 10 μ g/mL insulin, and 1 \times penicillin/streptomycin (all from Thermo Fisher) was used for maintenance and refreshed every 3 days. Automated stream acquisition of post deflection during CMW contraction was carried out on an Image Xpress Micro 4 using customized scripts. In compound dosing studies, dose-escalation schemes were employed so that each CMW would receive at most four escalating doses. Compounds were prepared at 10 \times final concentration in the medium and added to CMWs using liquid handling. A post-treatment video was recorded following a 3-min equilibration time after each dosing.

RNA sequencing

For bulk RNA-seq, hiPSC-CM RNA libraries were sequenced to a minimum depth of 30 million paired-end reads on an Illumina Hi-Seq4000. For scRNA-seq, 10–15 CMWs of each group (days 75–90) were harvested and pooled for papain dissociation. A volume targeting a capture rate of 8,000 cells was loaded on 10 \times Chromium

and libraries were sequenced on an Illumina NovaSeq6000. Computational data analysis is further described in [supplemental information](#).

SUPPLEMENTAL INFORMATION

Supplemental information can be found online at <https://doi.org/10.1016/j.stemcr.2022.11.008>.

AUTHOR CONTRIBUTIONS

G.H. and C.M.H. conceived and designed the study. G.H., A.B., D.L.W., T.M.Y., P.V., J.W., O.O., H.Z., O.F.V., and C.M.H. carried out experiments. D.L.W., A.B., O.F.V., and C.M.H. performed imaging analysis. T.M.Y., X.L., and J.A.Z. performed bioinformatic analysis. P.V. and A.B. performed MEA recordings and analysis. J.W. performed titin immunoblotting. J.D.R., C.-M.L., S.W., F.I.M., and J.J.H. provided resources and interpretation of the results. S.W. and C.M.H. supervised the study. G.H. and C.M.H. prepared the figures and wrote the original draft. All authors read and approved the final draft of the manuscript.

ACKNOWLEDGMENTS

We thank Jixin Cui and Yen-sin Ang for technical assistance with the MEA platform, Ning Li, Gongxin Liu, and Sridharan Rajamani for assistance and discussion on hiPSC-CM electrophysiology, and Huiren Zhao for immunoblotting. This study was fully funded by Amgen.

CONFLICT OF INTERESTS

D.L.W., T.M.Y., X.L., O.F.V., J.W., J.D.R., A.B., H.Z., C.L., S.W., and C.M.H. are employees of Amgen Inc. and own Amgen shares. G.H., J.A.Z., P.V., and O.O. were employees of Amgen when the experiments were conducted. F.I.M. and J.J.H. are employees of Cytokinetics Inc. and own Cytokinetics shares. Amgen and Cytokinetics hold intellectual property of the sarcomere modulators used in this study.

Received: October 8, 2021

Revised: November 10, 2022

Accepted: November 11, 2022

Published: December 15, 2022

REFERENCES

- Ahlberg, G., Refsgaard, L., Lundegaard, P.R., Andreasen, L., Ranthe, M.F., Linscheid, N., Nielsen, J.B., Melbye, M., Haunso, S., Sajadieh, A., et al. (2018). Rare truncating variants in the sarcomeric protein titin associate with familial and early-onset atrial fibrillation. *Nat. Commun.* 9, 4316.
- Bravo-San Pedro, J.M., Kroemer, G., and Galluzzi, L. (2017). Autophagy and mitophagy in cardiovascular disease. *Circ. Res.* 120, 1812–1824.
- Corden, B., Jarman, J., Whiffin, N., Tayal, U., Buchan, R., Sehmi, J., Harper, A., Midwinter, W., Lascelles, K., Markides, V., et al. (2019). Association of titin-truncating genetic variants with life-threatening



cardiac arrhythmias in patients with dilated cardiomyopathy and implanted defibrillators. *JAMA Netw. Open* 2, e196520.

Deacon, D.C., Happe, C.L., Chen, C., Tedeschi, N., Manso, A.M., Li, T., Dalton, N.D., Peng, Q., Farah, E.N., Gu, Y., et al. (2019). Combinatorial interactions of genetic variants in human cardiomyopathy. *Nat. Biomed. Eng.* 3, 147–157.

Eschenhagen, T., and Carrier, L. (2019). Cardiomyopathy phenotypes in human-induced pluripotent stem cell-derived cardiomyocytes—a systematic review. *Pflügers Arch.* 471, 755–768.

Fatkin, D., and Huttner, I.G. (2017). Titin-truncating mutations in dilated cardiomyopathy: the long and short of it. *Curr. Opin. Cardiol.* 32, 232–238.

Fomin, A., Gärtner, A., Cyganek, L., Tiburcy, M., Tuleta, I., Wellers, L., Folsche, L., Hobbach, A.J., von Frieling-Salewsky, M., Unger, A., et al. (2021). Truncated titin proteins and titin haploinsufficiency are targets for functional recovery in human cardiomyopathy due to TTN mutations. *Sci. Transl. Med.* 13, eabd3079.

Giacomelli, E., Meraviglia, V., Camprostrini, G., Cochrane, A., Cao, X., van Helden, R.W.J., Krotenberg Garcia, A., Mircea, M., Kostidis, S., Davis, R.P., et al. (2020). Human-iPSC-Derived cardiac stromal cells enhance maturation in 3D cardiac microtissues and reveal non-cardiomyocyte contributions to heart disease. *Cell Stem Cell* 26, 862–879.e11.

Gigli, M., Begay, R.L., Morea, G., Graw, S.L., Sinagra, G., Taylor, M.R.G., Granzier, H., and Mestroni, L. (2016). A review of the giant protein titin in clinical molecular diagnostics of cardiomyopathies. *Front. Cardiovasc. Med.* 3, 21.

Gramlich, M., Michely, B., Krohne, C., Heuser, A., Erdmann, B., Klaassen, S., Hudson, B., Magarin, M., Kirchner, F., Todiras, M., et al. (2009). Stress-induced dilated cardiomyopathy in a knock-in mouse model mimicking human titin-based disease. *J. Mol. Cell. Cardiol.* 47, 352–358.

Hinson, J.T., Chopra, A., Nafissi, N., Polacheck, W.J., Benson, C.C., Swist, S., Gorham, J., Yang, L., Schafer, S., Sheng, C.C., et al. (2015). HEART DISEASE. Titin mutations in iPSC cells define sarcomere insufficiency as a cause of dilated cardiomyopathy. *Science* 349, 982–986.

Hwang, P.M., and Sykes, B.D. (2015). Targeting the sarcomere to correct muscle function. *Nat. Rev. Drug Discov.* 14, 313–328.

Janssen, P.M.L. (2019). Myocardial relaxation in human heart failure: why sarcomere kinetics should be center-stage. *Arch. Biochem. Biophys.* 661, 145–148.

Lavandro, S., Chiong, M., Rothermel, B.A., and Hill, J.A. (2015). Autophagy in cardiovascular biology. *J. Clin. Invest.* 125, 55–64.

Lian, X., Zhang, J., Azarin, S.M., Zhu, K., Hazeltine, L.B., Bao, X., Hsiao, C., Kamp, T.J., and Palecek, S.P. (2013). Directed cardiomyocyte differentiation from human pluripotent stem cells by modulating Wnt/beta-catenin signaling under fully defined conditions. *Nat. Protoc.* 8, 162–175.

Linke, W.A., and Krüger, M. (2010). The giant protein titin as an integrator of myocyte signaling pathways. *Physiology* 25, 186–198.

Malik, F.I., Hartman, J.J., Elias, K.A., Morgan, B.P., Rodriguez, H., Brejc, K., Anderson, R.L., Sueoka, S.H., Lee, K.H., Finer, J.T., et al.

(2011). Cardiac myosin activation: a potential therapeutic approach for systolic heart failure. *Science* 331, 1439–1443.

McAfee, Q., Chen, C.Y., Yang, Y., Caporizzo, M.A., Morley, M., Babu, A., Jeong, S., Brandimarto, J., Bedi, K.C., Jr., Flam, E., et al. (2021). Truncated titin proteins in dilated cardiomyopathy. *Sci. Transl. Med.* 13, eabd7287.

McLendon, P.M., and Robbins, J. (2011). Desmin-related cardiomyopathy: an unfolding story. *Am. J. Physiol. Heart Circ. Physiol.* 301, H1220–H1228.

Pei, Z., Xiao, Y., Meng, J., Hudmon, A., and Cummins, T.R. (2016). Cardiac sodium channel palmitoylation regulates channel availability and myocyte excitability with implications for arrhythmia generation. *Nat. Commun.* 7, 12035.

Repetti, G.G., Toepfer, C.N., Seidman, J.G., and Seidman, C.E. (2019). Novel therapies for prevention and early treatment of cardiomyopathies. *Circ. Res.* 124, 1536–1550.

Ribeiro, A.J.S., Ang, Y.S., Fu, J.D., Rivas, R.N., Mohamed, T.M.A., Higgs, G.C., Srivastava, D., and Pruitt, B.L. (2015). Contractility of single cardiomyocytes differentiated from pluripotent stem cells depends on physiological shape and substrate stiffness. *Proc. Natl. Acad. Sci. USA* 112, 12705–12710.

Roberts, A.M., Ware, J.S., Herman, D.S., Schafer, S., Baksi, J., Bick, A.G., Buchan, R.J., Walsh, R., John, S., Wilkinson, S., et al. (2015). Integrated allelic, transcriptional, and phenomic dissection of the cardiac effects of titin truncations in health and disease. *Sci. Transl. Med.* 7, 270ra6.

Ronaldson-Bouchard, K., Ma, S.P., Yeager, K., Chen, T., Song, L., Sirabella, D., Morikawa, K., Teles, D., Yazawa, M., and Vunjak-Novakovic, G. (2018). Advanced maturation of human cardiac tissue grown from pluripotent stem cells. *Nature* 556, 239–243.

Rudolph, F., Fink, C., Hüttemeister, J., Kirchner, M., Radke, M.H., Lopez Carballo, J., Wagner, E., Kohl, T., Lehnart, S.E., Mertins, P., and Gotthardt, M. (2020). Deconstructing sarcomeric structure-function relations in titin-BioID knock-in mice. *Nat. Commun.* 11, 3133.

Ryder, D.J., Judge, S.M., Beharry, A.W., Farnsworth, C.L., Silva, J.C., and Judge, A.R. (2015). Identification of the acetylation and ubiquitin-modified proteome during the progression of skeletal muscle atrophy. *PLoS One* 10, e0136247.

Schafer, S., de Marvao, A., Adami, E., Fiedler, L.R., Ng, B., Khin, E., Rackham, O.J.L., van Heesch, S., Pua, C.J., Kui, M., et al. (2017). Titin-truncating variants affect heart function in disease cohorts and the general population. *Nat. Genet.* 49, 46–53.

Shintani-Domoto, Y., Hayasaka, T., Maeda, D., Masaki, N., Ito, T.K., Sakuma, K., Tanaka, M., Kabashima, K., Takei, S., Setou, M., and Fukayama, M. (2017). Different desmin peptides are distinctly deposited in cytoplasmic aggregations and cytoplasm of desmin-related cardiomyopathy patients. *Biochim. Biophys. Acta Proteins Proteom.* 1865, 828–836.

Sutcliffe, M.D., Tan, P.M., Fernandez-Perez, A., Nam, Y.J., Munshi, N.V., and Saucerman, J.J. (2018). High content analysis identifies unique morphological features of reprogrammed cardiomyocytes. *Sci. Rep.* 8, 1258.

Teerlink, J.R., Diaz, R., Felker, G.M., McMurray, J.J.V., Metra, M., Solomon, S.D., Adams, K.F., Anand, I., Arias-Mendoza, A.,



- Biering-Sørensen, T., et al. (2020). Cardiac myosin activation with omecamtiv mecarbil in systolic heart failure. *N. Engl. J. Med.* *384*, 105–116.
- Teerlink, J.R., Diaz, R., Felker, G.M., McMurray, J.J.V., Metra, M., Solomon, S.D., Biering-Sørensen, T., Böhm, M., Bonderman, D., Fang, J.C., et al. (2021). Effect of ejection fraction on clinical outcomes in patients treated with omecamtiv mecarbil in GALACTIC-HF. *J. Am. Coll. Cardiol.* *78*, 97–108.
- Teerlink, J.R., Felker, G.M., McMurray, J.J.V., Solomon, S.D., Adams, K.F., Jr., Cleland, J.G.F., Ezekowitz, J.A., Goudev, A., MacDonald, P., Metra, M., et al. (2016). Chronic oral study of myosin activation to increase contractility in heart failure (COSMIC-HF): a phase 2, pharmacokinetic, randomised, placebo-controlled trial. *Lancet* *388*, 2895–2903.
- Thavandiran, N., Hale, C., Blit, P., Sandberg, M.L., McElvain, M.E., Gagliardi, M., Sun, B., Witty, A., Graham, G., Do, V.T.H., et al. (2020). Functional arrays of human pluripotent stem cell-derived cardiac microtissues. *Sci. Rep.* *10*, 6919.
- Verdonschot, J.A.J., Hazebroek, M.R., Derks, K.W.J., Barandiarán Aizpurua, A., Merken, J.J., Wang, P., Bierau, J., van den Wijngaard, A., Schalla, S.M., Abdul Hamid, M.A., et al. (2018). Titin cardiomyopathy leads to altered mitochondrial energetics, increased fibrosis and long-term life-threatening arrhythmias. *Eur. Heart J.* *39*, 864–873.
- Walsh, R., Thomson, K.L., Ware, J.S., Funke, B.H., Woodley, J., McGuire, K.J., Mazzarotto, F., Blair, E., Seller, A., Taylor, J.C., et al. (2017). Reassessment of Mendelian gene pathogenicity using 7, 855 cardiomyopathy cases and 60, 706 reference samples. *Genet. Med.* *19*, 192–203.
- Wan, E., Abrams, J., Weinberg, R.L., Katchman, A.N., Bayne, J., Zakharov, S.I., Yang, L., Morrow, J.P., Garan, H., and Marx, S.O. (2016). Aberrant sodium influx causes cardiomyopathy and atrial fibrillation in mice. *J. Clin. Invest.* *126*, 112–122.
- Wang, L., Yu, P., Zhou, B., Song, J., Li, Z., Zhang, M., Guo, G., Wang, Y., Chen, X., Han, L., and Hu, S. (2020). Single-cell reconstruction of the adult human heart during heart failure and recovery reveals the cellular landscape underlying cardiac function. *Nat. Cell Biol.* *22*, 108–119.
- Ware, J.S., and Cook, S.A. (2018). Role of titin in cardiomyopathy: from DNA variants to patient stratification. *Nat. Rev. Cardiol.* *15*, 241–252.
- Yang, X., Pabon, L., and Murry, C.E. (2014). Engineering adolescence: maturation of human pluripotent stem cell-derived cardiomyocytes. *Circ. Res.* *114*, 511–523.